THE MAGNETIC FIELD OF THE INTERMEDIATE POLAR RE 0751+14

H. VÄTH, 1,2 G. CHANMUGAM, 2 AND J. FRANK 2 Received 1995 March 6; accepted 1995 July 28

ABSTRACT

Piirola, Hakala, & Coyne modeled the optical/IR light curve of RE 0751+14 assuming a uniform shock structure and neglecting the hard X-ray emission. In this paper, we model the light curves at optical/IR and hard X-ray wavelengths and include the effects of the shock structure.

We base our model on accretion onto a white dwarf with a displaced magnetic dipole for a range of likely white dwarf masses. We find that the observed intensity variations of X-rays and in the I band over one spin period largely determine the position of the emission regions. Furthermore, the observed maximum X-ray flux constrains the specific accretion rate. We deduce that the magnetic field at the pole is likely to be in the range 9-21 MG, which is consistent with the estimates of Piirola et al. It had been proposed previously that there must exist asynchronous rotators with sufficiently strong magnetic fields such that the binaries will evolve into AM Her binaries (Chanmugam & Ray; King, Frank, & Ritter). With this deduced high magnetic field, RE 0751+14 is the most likely example of such a system known to date.

Subject headings: accretion, accretion disks — novae, cataclysmic variables — stars: individual (RE 0751+14) — stars: magnetic fields — X-rays: stars

1. INTRODUCTION

Cataclysmic variables (CVs) are close binary systems in which a white dwarf star accretes matter from a red dwarf companion, usually via an accretion disk (Frank, King, & Raine 1992). About $\frac{1}{4}$ of all known CVs (Ritter & Kolb 1995) have a magnetic field sufficiently strong to disrupt the accretion disk either partially or completely and are known as magnetic CVs. Two classes of magnetic CVs have been distinguished (e.g., Chanmugam 1992). One of these is formed by the synchronous systems in which the spin period of the white dwarf $P_{\rm spin} \approx P_{\rm orb}$, where $P_{\rm orb}$ is the orbital period. These systems are also known as AM Herculis binaries after their prototype, or polars (Cropper 1990) because they emit strong $(\sim 10\%)$ phase-dependent linear and circular polarization in the optical and IR. This polarization is caused by cyclotron radiation from the vicinity of the accretion shock that is formed near the surface of the white dwarf. From this and the detection of Zeeman and cyclotron features, it follows that the white dwarf has a strong magnetic field $B \sim 10-70$ MG. In addition, most of these binaries have short orbital periods (<4 hr). It is this short period, and hence short orbital separation, combined with the strong magnetic field which causes the synchronous rotation of the white dwarf (e.g., Joss, Katz, & Rappaport 1979; Lamb et al. 1983; Campbell 1990; King, Frank, & Whitehurst 1990; Katz 1991; Wu & Wickramasinghe 1993). In the AM Herculis-type system V1500 Cyg, in which $P_{\rm spin}$ is lower than $P_{\rm orb}$ by about 1.8% (Stockman, Schmidt, & Lamb 1988), a spin-down of the white dwarf was discovered by Schmidt & Stockman (1991), and the system should synchronize at the current rate in 170 ± 8 yr (Schmidt, Liebert, & Stockman 1995). As a consequence of the synchronism, all emission from the X-ray to the IR band varies with $P_{\rm orb}$.

A second class of magnetic CVs consists of the asynchronous rotators in which the spin period is much shorter than the orbital period. These in general do not emit polarized optical radiation, so that there is no direct evidence of a magnetic field. Nevertheless, one requires $B \gtrsim 5 \times 10^4$ G to channel the accretion flow onto the polar caps of the white dwarf, thereby producing radiation at optical and X-ray wavelengths modulated at the rotation period of the white dwarf. The qualitative shape of the X-ray light curve is approximately sinusoidal. With the assumption that hard X-rays are produced by optically thin bremsstrahlung emission, King & Shaviv (1984) concluded that the accretion occurs onto a larger area of the white dwarf than in synchronous rotators. This class of systems has been further subdivided. Systems with $P_{\rm spin}/P_{\rm orb}\sim 0.1$ are known as intermediate polars (IPs; e.g., Warner 1985). In addition, a small class of asynchronous systems known as DQ Her binaries has been identified. These systems have similar properties to the IPs, but $P_{\rm spin}/P_{\rm orb} \ll 0.1$, and the X-ray emission is weak or completely absent. Note that some authors refer to all asynchronous rotators as DQ Her binaries (Patterson 1994).

A straightforward explanation for the asynchronism and the general absence of polarization from the asynchronous rotators is to assume that $B \lesssim 1$ MG (Lamb & Patterson 1983; Wickramasinghe, Wu, & Ferrario 1991). Chanmugam & Ray (1984) pointed out that most of these systems have longer orbital periods than the AM Her binaries, and hence some of them may have strong fields ($\sim 10 \text{ MG}$) and yet remain asynchronous because of their larger orbital separation. They also suggested that the asynchronous rotators would evolve to shorter orbital periods as a result of angular momentum losses (Verbunt & Zwaan 1981; Spruit & Ritter 1983; Rappaport, Verbunt, & Joss 1983) and become synchronized if $B \gtrsim 3$ MG (see also Lamb & Melia 1987). King, Frank, & Ritter (1985) suggested that these two classes should have magnetic fields of the same order of magnitude in order to explain the orbital period distribution of magnetic CVs, and they also supported an evolution of asynchronous into synchronous rotators. This raises the question as to why no polarization is observed in the

¹ Institut für Astronomie und Astrophysik der Universität, 24098 Kiel, Germany; supas097@astrophysik.uni-kiel.d400.de.

² Department of Physics and Astronomy, Louisiana State University, Baton Rouge, LA 70803-4001; chanmuga, frank@rouge.phys.lsu.edu.

asynchronous rotators, and it has been suggested that this is attributable to dilution effects. Furthermore, if asynchronous rotators with sufficiently strong magnetic fields evolve into AM Her binaries, then one would expect to find some systems with $P_{\rm spin}/P_{\rm orb}\sim 0.1$ like IPs but which also show polarization in the optical/IR. The evolutionary scenario was supported by the discovery of weak $(-0.239 \pm 0.030\%)$ circular polarization in the I band (centered at 8250 Å) in BG CMi by Penning, Schmidt, & Liebert (1986). The magnetic nature of this object was confirmed by West, Berriman, & Schmidt (1987), who discovered $-1.74 \pm 0.26\%$ circular polarization in the J band. Yet this object has $P_{\rm spin} = 15.3$ minutes and $P_{\rm orb} = 3.23$ hr and therefore is classified as an IP. Models for polarization by Chanmugam et al. (1990) gave a field strength B = 3-10 MG with a preferred value of $B \approx 4$ MG. This is above the critical value of about 3 MG for synchronization. However, since this value depends on other physical parameters such as the magnetic moment and hence radius of the white dwarf, it is uncertain whether this system will synchronize.

Recently, a second IP, RE 0751 + 14 (Mason et al. 1992), was discovered to emit optically polarized radiation (Rosen, Mittaz, & Hakala 1993; Piirola, Hakala, & Coyne 1993). Hard X-ray observations with Ginga showed modulations that implied $P_{\rm spin} = 13.9$ minutes (Mason et al. 1992). Rosen et al. (1993) obtained optical spectroscopy, photometry, and polarimetry of this binary and argued that the 14.5 minute modulation in the B band was caused by a beat period of the spin period with an orbital period of 5.3 hr. Piirola et al. (1993) made simultaneous UBVRI linear and circular polarimetry and photometry and found variable linear and circular polarization. They fitted the maximum polarized flux to cyclotron emission models (Wickramasinghe & Meggitt 1985; Wickramasinghe et al. 1991) for different values of B, the temperature T, and the dimensionless plasma parameter $\Lambda = \omega_p^2 L/\omega_c c = 6 \times 10^7 (L/10^7 \text{ cm}) (n/10^{16} \text{ cm}^{-3}) (B/10 \text{ MG})^{-1}$. Here $\omega_p = (4\pi ne^2/m)^{1/2} = 5.64 \times 10^{12} (n/10^{16} \text{ cm}^{-3})^{1/2} \text{ s}^{-1}$ is the plasma frequency, $\omega_c = eB/mc = 1.76 \times 10^{14} (B/10 \text{ MG})$ s^{-1} is the cyclotron frequency, n is the electron number density, and L is the characteristic length of the cyclotron emission region. They deduced that B = 8-18 MG, kT = 10-20 keV, and $\Lambda \approx 10^6 - 10^8$ (the higher value of Λ corresponds to the lower B). This suggests that the system is much more likely to synchronize than BG CMi.

The aim of this paper is to constrain more strongly the magnetic field strength of RE 0751+14. For this we include in our model, in addition to the optical/IR emission, the observed hard X-ray emission (Mason et al. 1992) and include the vertical structure of the shock, neither of which was taken into account by Piirola et al. (1993). The geometry of the emission regions in our model is that which results from accretion onto a white dwarf with a displaced dipole. In § 2 we describe our model and explain the differences between it and the model of Piirola et al. (1993), and we describe how we solve the radiative transfer. In § 3 we present the results of our calculations and fit them to the observational data that were obtained at hard X-ray energies by Mason et al. (1992) and at optical/IR wavelengths by Piirola et al. (1993), and we deduce that the magnetic field at the pole is likely to be in the range 9-21 MG.

2. THE ACCRETION SHOCK IN RE 0751+14

Piirola et al. (1993) were able to estimate B and Λ of the accretion region of RE 0751+14 by fitting the observed circularly polarized flux F_c^{obs} . For this they used the uniform tem-

perature models of Wickramasinghe & Meggitt (1985) and the extended emission region model of Wickramasinghe et al. (1991). Furthermore, Piirola et al. (1993) could qualitatively fit the variation over one spin period of the optical flux $F^{\rm obs}$, the degree of linear and circular polarization $P_l^{\rm obs}$ and $P_c^{\rm obs}$, and the position angle $\chi^{\rm obs}$ of linear polarization. They did this by calculating the Stokes parameters from individual points of the emission regions on the white dwarf using the models of Wickramasinghe & Meggitt (1985). Hence, they assumed that the radiation from the different points can be obtained independently, i.e., that the shock height is small in comparison to the size of the emission regions. Furthermore, they assumed that the magnetic field in the accretion regions is radial.

Here we fit the observations at optical/IR and hard X-ray wavelengths by assuming that the magnetic field of the white dwarf results from a displaced dipole. Its magnetic field can be written as $B(r) = (B_0/2)(R/r)^3(3 \cos \Theta \sin \Theta \cos \Phi, 3 \cos \Theta)$ $\sin \Theta \sin \Phi$, $3 \cos^2 \Theta - 1$) with the polar coordinates r, Θ , and Φ measured from the displaced dipole, and where R is the radius of the white dwarf. Determining B_0 is the main focus of this work. The geometry of the emission region is determined mainly by the position of the dipole with respect to the center of the white dwarf (given by $r_{\rm dd}$, $\theta_{\rm dd}$, and $\phi_{\rm dd}$ in spherical coordinates) and by the extent of the coupling region in which matter originating from the secondary threads the magnetic field of the white dwarf. As the magnetic field increases at smaller radii, the magnetic pressure will eventually overcome the gas stresses. This will occur at the magnetospheric radius (e.g., Frank et al. 1992)

$$r_m = 5.1 \times 10^8 (\dot{M}/10^{16} \text{ g s}^{-1})^{-2/7} (M/M_{\odot})^{-1/7} \times (\mu/10^{30} \text{ G cm}^3)^{4/7} \text{ cm}, (1)$$

where \dot{M} is the accretion rate, M is the mass of the white dwarf, and $\mu = BR^3$ is the magnetic moment. After coupling, the matter flows along field lines to the magnetic pole of the white dwarf. If, for simplicity, the white dwarf is assumed to have a centered and inclined dipole, then material linking to the field at a position (r, ϕ) in the orbital plane will land on the surface at a magnetic colatitude ϵ given by (Wickramasinghe 1988)

$$\sin \epsilon = (R/r)^{1/2}(1 - \sin^2 \delta \cos^2 \phi)^{1/2}$$
. (2)

Here r is the distance from the center of the white dwarf, ϕ is the azimuthal angle measured from the projection of the magnetic axis onto the orbital plane, and δ is the inclination of the dipole axis to the rotation axis of the white dwarf (the latter will be parallel to the orbital axis after only a small amount of matter has accreted onto the white dwarf). If now the dipole is displaced and its displacement from the white dwarf center is not large and $r \gg R$, we can use equation (2) in order to calculate ϵ . However, ϵ is then the magnetic colatitude of this accretion point measured on a sphere centered on the displaced dipole. The radius of this sphere is equal to the distance between the dipole and the accretion point, which is located on the surface of the white dwarf. The actual latitude and longitude of this point measured on the white dwarf surface can be calculated for given $r_{\rm dd}/R$, $\theta_{\rm dd}$, $\phi_{\rm dd}$, δ , r/R, and ϕ using spherical geometry. The exact extent of the coupling region is not known as the magnetospheric radius (eq. [1]) is only an estimate. Rather than a fixed radius, one can expect a range of radii over which matter on average will couple to the magnetic field. Furthermore, because of the centrifugal barrier (Patterson 1994), matter may only be able to couple to the magnetic field

lines at significantly smaller radii than r_m . A lower limit for the coupling region is the corotation radius

$$r_c = (GMP_{\rm spin}^2/4\pi^2)^{1/3} \tag{3}$$

at which a Keplerian disk has an orbital period equal to the spin period of the white dwarf. We will use this radius as the inner coupling radius, even though it is uncertain. The outer radius is a free parameter in our calculations and is expressed in multiples of r_c , whereby we expect that it is not many times r_c . We examine in § 3 how important the extent of the coupling region is for the resulting estimate of B_0 .

For the structure of the accretion shock, we have to know the specific accretion rate \dot{m} , the mass M of the white dwarf, and R. Therefore, we need a mass-radius relation, and we choose here the Nauenberg (1972) relation for a pure carbon white dwarf. We calculate the shock structure with the closedintegral formula of Wu, Chanmugam, & Shaviv (1994), but for this we have to assume that the shock height $x_s \ll R$. For \dot{m} , we assume that it is constant across the emission region, and we use the same value for both accretion poles. One would suppose that the accretion rate is much higher in the part of the accretion region with $|\phi| < 90^{\circ}$ than in the part with $|\phi| > 90^{\circ}$, as long as the magnetic axis is clearly not perpendicular to the orbital plane. We select a range of ϕ where $\dot{m} \neq 0$ that can reproduce the observed light curves, but we use the same range of ϕ for both accretion poles. An additional free parameter, which is critical for the shape of the light curves, is the inclination i of the white dwarf rotation axis with the line of sight.

We assume that the X-rays are caused by optically thin bremsstrahlung emission. Its total emissivity is given by Rybicki & Lightman (1979) as

$$\epsilon_{\rm br} = 1.4 \times 10^{-27} T^{1/2} n^2 g_{\rm ff}(T) \,{\rm erg s^{-1} \, cm^{-3}}$$
, (4)

where $g_{\rm ff} \sim 1$ is the Gaunt factor.

To describe polarized radiation we use the Stokes parameters. Then the transfer of radiation through matter is described by the three opacities κ , q, and v, and by the Faraday mixing coefficients f and h (e.g., Meggitt & Wickramasinghe 1982). Because the calculation of κ , q, and v requires much computing time, we calculate accurate tables of these three opacities for different temperatures, angles θ between the magnetic field and the line of sight, and frequency ratios $s = \omega/\omega_c$ before solving the radiative transfer and then interpolate from these tables. The computation and accuracy of the cyclotron opacities are described by Väth & Chanmugam (1995). We do

not tabulate the Faraday mixing coefficients, as they are given by simple analytical expressions (Pacholczyk 1977; Meggitt & Wickramasinghe 1982). We also include the free-free opacities in our calculations. The analytical expressions are given by Pacholczyk (1977) and Wickramasinghe & Meggitt (1985). The formal solution of the radiative transfer equation as used here is derived by Pacholczyk (1977) with some corrections by Väth (1994a). The radiative transfer calculations were performed on the MasPar MP-1, which is a single instruction multiple data (SIMD) computer with 8192 or 16,384 processors depending on its configuration. See Väth (1994a, b) for details.

3. DISCUSSION

From Ginga observations, Ishida (1991) concluded that the temperature in the hard X-ray emission region is $kT = 20.1 \pm 7.7$ keV. The temperature of a strong shock that results from free-fall accretion and is located right at the surface of the white dwarf is given as

$$kT = \frac{3}{8} \frac{GM}{R} \mu m_{\rm H},\tag{5}$$

where $\mu=0.62$ is the mean molecular weight for solar abundances of the accreting gas and $m_{\rm H}$ is the mass of the hydrogen atom. Ishida (1991) compared this temperature to the lower estimate of the observed temperature and deduced M=0.31 M_{\odot} with the mass-radius relation $R=5.5\times10^8(M/M_{\odot})^{-1/3}$. This relation is, however, quite inaccurate compared to the one by Nauenberg (1972), which we use here. In Table 1 we list the temperature T_s , the shock height x_s , and the number density n_s in the postshock region at the shock surface (indicated by the subscript) for different M and \dot{m} following Wu et al. (1994). If we compare the observed temperature with T_s , we obtain a range M=0.48-0.78 M_{\odot} . From Table 1 one can see that a range of M=0.4-0.8 M_{\odot} is reasonable, and we will use it in the following.

In Table 1 we also list the parameter

$$\epsilon_{s} = \frac{t_{\rm br}}{t_{\rm cyc}} \bigg|_{s} \approx 9 \times 10^{-3} \bigg(\frac{B}{10 \text{ MG}} \bigg)^{2.85} \bigg(\frac{T_{s}}{10^{8} \text{ K}} \bigg)^{2} \times \bigg(\frac{10^{16} \text{ cm}^{-3}}{n_{s}} \bigg)^{1.85} \bigg(\frac{10^{7} \text{ cm}}{x_{s}} \bigg)^{0.85}, \tag{6}$$

where $t_{\rm br}$ and $t_{\rm cyc}$ are the timescales for bremsstrahlung cooling and optically thick cyclotron cooling in the postshock region,

TABLE 1
Accretion Column on a Magnetic White Dwarf

<i>M</i> (<i>M</i> _⊙)	R (cm)	(g cm ⁻² s ⁻¹)	kT _s (keV)	(cm)	n _s (cm ⁻³)	ϵ_s
0.4	1.1×10^{9}	0.10	9.5	1.8×10^{8}	7.7×10^{14}	0.11
	1.1×10^{9}	0.50	9.5	3.7×10^{7}	3.8×10^{15}	0.02
	1.1×10^{9}	1.00	9.5	1.9×10^{7}	7.7×10^{15}	0.01
0.5	9.7×10^{8}	0.10	13.3	2.7×10^{8}	6.5×10^{14}	0.21
	9.7×10^{8}	0.50	13.3	5.9×10^{7}	3.2×10^{15}	0.04
	9.7×10^{8}	1.00	13.3	3.2×10^{7}	6.5×10^{15}	0.02
0.6	8.8×10^{8}	0.50	17.8	8.7×10^{7}	2.8×10^{15}	0.06
	8.8×10^{8}	1.00	17.8	4.8×10^{7}	5.6×10^{15}	0.03
0.7	7.9×10^{8}	0.50	23.0	1.2×10^{8}	2.5×10^{15}	0.10
	7.9×10^{8}	1.00	23.0	7.0×10^{7}	4.9×10^{15}	0.05
0.8	7.1×10^{8}	0.50	29.3	1.5×10^{8}	2.2×10^{15}	0.17
	7.1×10^{8}	1.00	29.3	9.8×10^{7}	4.4×10^{15}	0.07

respectively (optically thin cyclotron cooling only becomes important at much higher magnetic field strengths than what we expect for RE 0751+14). If $\epsilon_s \ll 1$, then bremsstrahlung cooling is dominant (Wu et al. 1994). For the values in Table 1 we use B=10 MG, which is what we expect approximately according to Piirola et al. (1993). We restrict our discussion to those parameters which lead to $x_s \ll R$ for self-consistency.

Next we determine the geometry of the emission regions that can reproduce the main features of the observed optical and X-ray light curves (Fig. 1). Mason et al. (1992) noted that the hard X-ray light curve at low energies (<10 keV) shows a dip at a phase when the flux in the high-energy range peaks. This energy-dependent component of the light curve was attributed by them to absorption of the X-ray photons by the accretion stream. The absorption cross section decreases with increasing

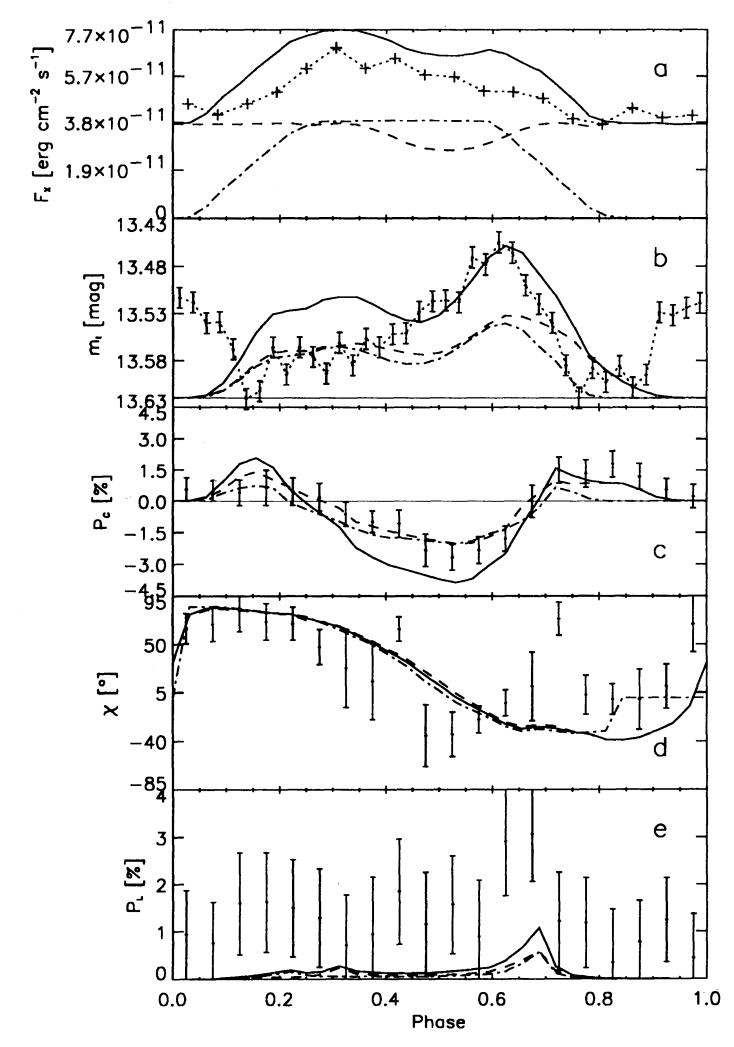


Fig. 1.—The observed light curves of RE 0751 + 14 and the fit of the light curves for $M=0.8~M_{\odot}$, $\dot{m}=0.4~{\rm g~cm^{-2}~s^{-1}}$, $B_0=12~{\rm MG}$, and an outer coupling radius of $1.5r_c$ for the northern pole (dashed), the southern pole (dashed), and both poles combined (solid). (a) The X-ray flux in the $10-20~{\rm keV}$ regime, which is adapted from Mason et al. (1992) (crosses and dotted line), and the calculated total X-ray flux. The observed X-ray flux is normalized such that its minimum agrees with the minimum of the calculated X-ray flux. (b-e) Intensity, degree of circular polarization, position angle, and degree of linear polarization, respectively, for the I band. The observations (error bars, dotted) are adapted from Piirola et al. (1993). An unpolarized, phase-independent background has been added to the calculated cyclotron radiation such that the maximum calculated cyclotron flux is 16% of the background.

energy of the X-ray photons. Therefore, the radiation at high energies more closely corresponds to the X-ray light curve of the shock itself, which is what we model here. For that reason, we try to fit by our calculations the shape of the X-ray light curve at energies in the 10–20 keV regime as measured by Mason et al. (1992). In their optical observations, Piirola et al. (1993) found the highest degree of linear and circular polarization in the *I* band, and hence we fit the calculated optical/IR light curve to the observations in this wavelength band. We emphasize, however, that the observations at X-ray and optical wavelengths were not done simultaneously. The alignment of these observations shown in Figure 1 is only based on what fits our calculations best.

Like Piirola et al. (1993), we conclude from the negative and positive degree of circular polarization that accretion occurs onto two opposite poles. In addition, as the hard X-rays are observed over the entire spin period, at least one emission region must be visible at all times. The smooth variation of γ between values less than 180° apart restricts the values of δ and i to $\delta < i$ (Piirola et al. 1993). For the fit shown in Figure 1, we have $M = 0.8 M_{\odot}$, $\dot{m} = 0.4 \text{ g cm}^{-2} \text{ s}^{-1}$, and $B_0 = 12 \text{ MG}$. The position of the displaced dipole is given as $r_{\rm dd}/R = 0.19$, $\theta_{\rm dd} =$ 81°, and $\phi_{\rm dd} = 203^{\circ}$, and we have $\delta = 25^{\circ}$ and $i = 70^{\circ}$. The coupling region has a radius $r = (1-1.5)r_c$. Accretion occurs for $-15^{\circ} \le \phi \le 75^{\circ}$. In order to be able to quantitatively compare the calculated optical light curve with the observations, we added to the cyclotron flux an unpolarized phase-independent background. For the fit shown in Figure 1, the maximum calculated cyclotron flux in the I band is 16% of the background flux. The asymmetric peaks of both the optical and X-ray light curve restrict the values of δ and i, but they cannot be determined more accurately than to about $\pm 10^{\circ}$ as a result of the large error bars. These peaks in the optical and at X-ray energies also require an offset dipole in our model of the emission regions. However, we could shift its position from the one used in Figure 1 by about 0.05R in any direction and would still get a fit of equal quality. The range of ϕ has to be clearly smaller than π , as the optical and X-ray peaks would be overly broad otherwise. Therefore, we choose a range of $\pi/2$. The peak in the linear polarization determines the offset of ϕ to about $\pm 10^{\circ}$. The fit to the observed light curves for a coupling between r_c and $2r_c$ with all the other parameters unchanged is similar to the one shown in Figure 1. The values of M, \dot{m} , and B_0 do not strongly influence the shape of the light curves as long as the calculated cyclotron emission in the I band is marginally optically thin.

One can see that differences between the calculated light curves and the observations remain. However, the noise in the observations, particularly for the degree of linear polarization, is very large. In addition, our model contains certain simplifications. Therefore, we content ourselves with a fit of this quality. In particular, a secondary peak in the *I* band occurs around phase 0, which is fitted neither by us nor by Piirola et al. (1993). Because no polarization is observed at this phase, this peak is probably not caused by cyclotron radiation. This feature also shows that the unpolarized background is not phase independent, as we assume when we compare the observations to the calculations. Our lack of knowledge about the phase dependence of the unpolarized background is another reason why we are not trying to fit every detail of the observed light curves.

If we know the distance to this system, we can also compare the flux emitted by our model at 8250 Å with the observations

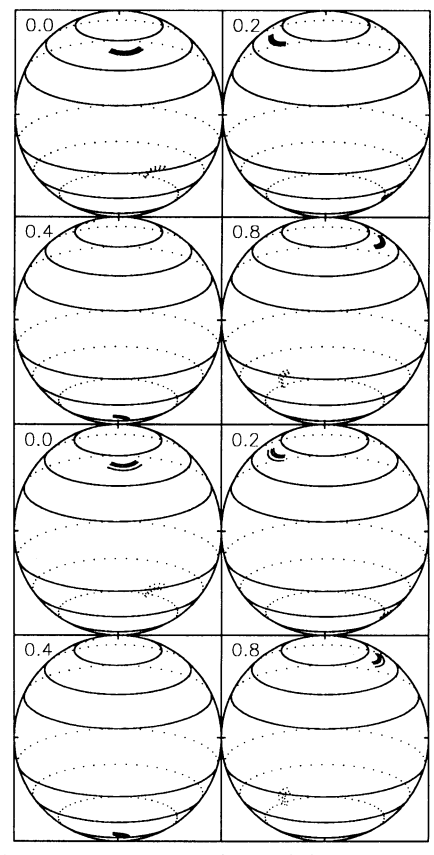


Fig. 2.—The apparent movement of the emission regions across the white dwarf disk with $M=0.8~M_{\odot}$. The upper rows are for a model in which matter couples to the magnetic field at radii between $1-1.5r_c$, while in the lower rows matter coupling occurs between $1-2r_c$. The numbering of the phases agrees with that in Fig. 1. Visible regions are solid, while hidden regions are dotted. The lines of constant latitude are for 25°, 45°, and 65° in the northern (upper) hemisphere and for 15°, 35°, and 55° in the southern (lower) hemisphere, similar to Fig. 5 of Piirola et al. (1993).

by Mason et al. (1992; see their Fig. 2). We use in the following a distance of 400 pc for the system as estimated by Patterson (1994), but since this is uncertain we do not try to compare calculated to observed fluxes to better than about a factor of 2. For the model used in Figure 1, for which the cyclotron emission is marginally optically thin, the maximum optical flux is 9.2×10^{-15} ergs cm⁻² s⁻¹ Å⁻¹. This is consistent with the observations given the uncertainties.

In Figure 2 we show the apparent positions of the emission regions as they move across the white dwarf disk in order to

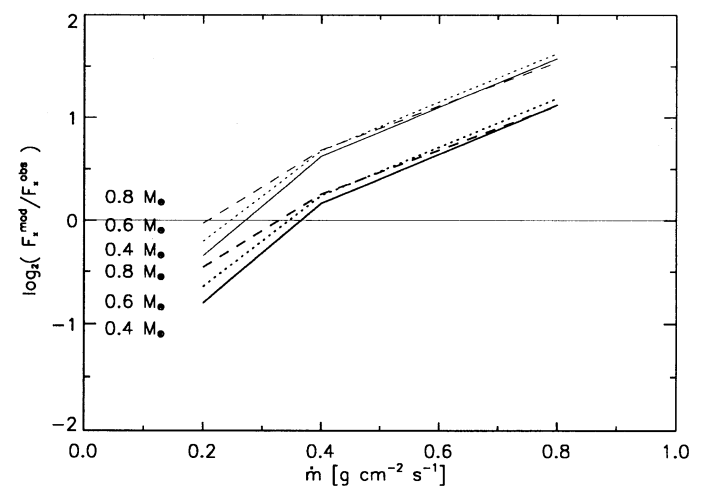


Fig. 3.—Comparison of the calculated X-ray flux F_x^{mod} for a distance of 400 pc with the observed X-ray flux $F_x^{\text{obs}} = 6.4 \times 10^{-11} \, \text{ergs cm}^{-2} \, \text{s}^{-1}$ (Ishida 1991) for different specific accretion rates \dot{m} and white dwarf masses of $0.4 \, M_{\odot}$ (solid), $0.6 \, M_{\odot}$ (dotted), and $0.8 \, M_{\odot}$ (dashed). The thick lines are for a coupling region between $1-1.5r_c$, and the thin lines correspond to a coupling region between $1-2r_c$. Note that an agreement of the calculated X-ray flux with the observations within a factor of 2 means that $-1 \leq \log_2 \left(F_x^{\text{mod}}/F_x^{\text{obs}}\right) \leq 1$.

illustrate the geometry of the emission regions. The phases listed in this figure are identical to the phases used in Figure 1. Therefore, these two figures can be used together in order to easily visualize how the calculated behavior at X-ray and optical wavelengths comes about. By comparing this figure to Figure 5 of Piirola et al. (1993), one immediately sees a difference between the two models. The surface fraction of the white dwarf that is covered by these two emission regions is about 6% in Piirola et al. (1993) as deduced from their Figure 5, while in our calculations it is only 0.64% for $r = (1-2)r_c$ and M = 0.4 M_{\odot} , and it is even smaller for all other models. This means that in our computations, as in AM Her, accretion occurs onto a smaller region of the white dwarf surface than in the asynchronous rotators.

Next, in Figure 3 we show the ratio of the calculated maximum X-ray flux to the observed frequency integrated X-ray flux. The latter is given as $F_x^{\text{obs}} = 6.4 \times 10^{-11} \text{ ergs cm}^{-2} \text{ s}^{-1}$ by Ishida (1991) when integrated from 1.2 to 37.4 keV. From this figure we can see that values of $\dot{m} = 0.2$, 0.4, and 0.8 g cm⁻² s⁻¹ generally fit the observed flux to within a factor of 2, and only in the case of $\dot{m} = 0.8$ g cm⁻² s⁻¹ and an extended coupling region do we obtain an X-ray flux that is too high.

TABLE 2
Possible Range of Magnetic Field Strengths

$M \atop (M_{\odot})$	$(g cm^{-3} s^{-1})$	B _{lower} (MG)	B _{upper} (MG)	μ (G cm ³)	r _m (cm)	r _c (cm)
0.4	0.2	≃16	<22	2.4×10^{34}	1.7×10^{11}	9.8×10^{9}
	0.4	≃ 14	< 20	2.1×10^{34}	1.3×10^{11}	
	0.8	>12	< 18	1.9×10^{34}	1.0×10^{11}	
0.6	0.2	≃ 14	< 20	1.1×10^{34}	1.3×10^{10}	1.1×10^{10}
	0.4	>10	< 16	8.7×10^{33}	9.0×10^{10}	
	0.8	>8	< 14	7.4×10^{33}	6.7×10^{10}	
0.8	0.2	>12	$\simeq 18$	5.5×10^{33}	9.8×10^{10}	1.2×10^{10}
	0.4	>10	< 16	4.6×10^{33}	7.3×10^{10}	
	0.8	>8	< 12	3.6×10^{33}	5.1×10^{10}	

412

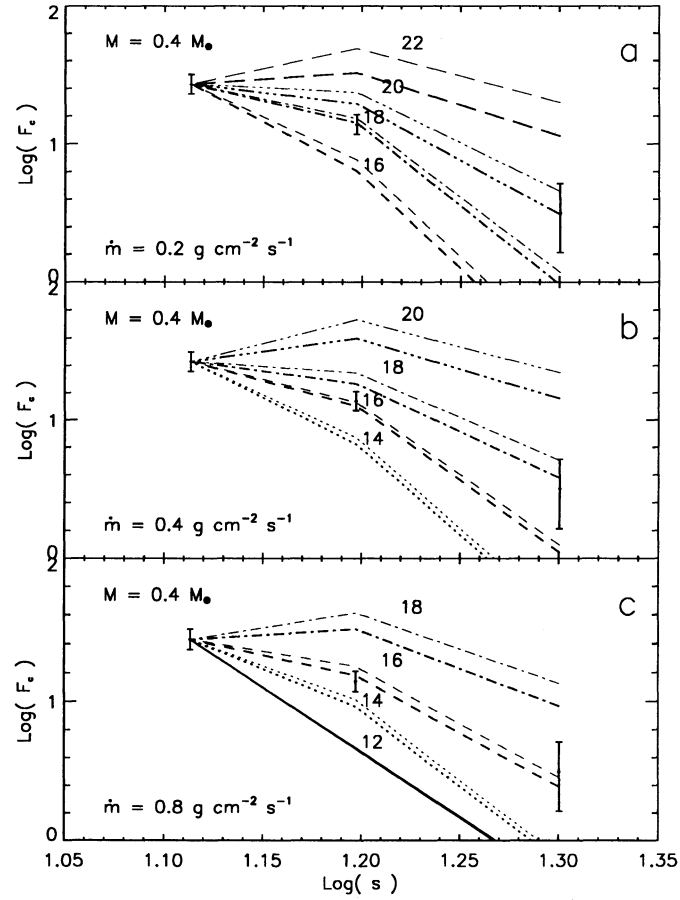


Fig. 4.—Fit of the calculated to the observed maximum circularly polarized flux for $M=0.4~M_{\odot}$. The observed data points (error bars) are extracted from Fig. 3 of Piirola et al. (1993) and correspond to the I, R, and V band (left to right). All curves have been normalized to the observed flux in the I band. The frequency is given in terms of the frequency ratio s with a magnetic field of 8 MG similar to Piirola et al. (1993). The individual curves are for models with magnetic fields of $B_0 = 12$ MG (solid), $B_0 = 14$ MG (dotted), $B_0 = 16$ MG (dashed), $B_0 = 18$ MG (dash-dotted), $B_0 = 20$ MG (dash-triple-dotted), and $B_0 = 22$ MG (long-dashed) (a) for $\dot{m} = 0.2$ g cm⁻² s⁻¹, (b) for $\dot{m} = 0.4$ g cm⁻² s⁻¹, and (c) for $\dot{m} = 0.8$ g cm⁻² s⁻¹. The thick lines are for a coupling region between $1-1.5r_c$, and the thin lines correspond to a coupling region between $1-2r_c$.

However, because of possible absorption of hard X-ray photons, the observed X-ray flux may well be too low. Furthermore, for these values of \dot{m} the shock is mostly dominated by bremsstrahlung cooling, and the shock height is small enough to justify the use of the closed integral formula for the shock structure (see Table 1). Only for $M=0.8~M_{\odot}$ and $\dot{m}=0.2$ g cm⁻² s⁻¹ are these conditions not fulfilled anymore.

Having determined a reasonable range for \dot{m} , we can calculate the maximum circularly polarized flux in the V, R, and Iband for different magnetic field strengths B_0 and compare it to F_c^{obs} (Piirola et al. 1993). In Figures 4, 5, and 6 we show our results for $M = 0.4, 0.6, \text{ and } 0.8 M_{\odot} \text{ and } \dot{m} = 0.2, 0.4, \text{ and } 0.8 \text{ g}$ cm⁻² s⁻¹. In each figure we show the fit for a coupling region extending to $1.5r_c$ and for a coupling region extending to $2r_c$. One can see that the exact extent of the coupling region does not have a significant influence on the resulting slope of the circularly polarized flux and hence the resulting estimates for the magnetic field. Furthermore, we find that the position of the dipole does not influence strongly the resulting B_0 either.

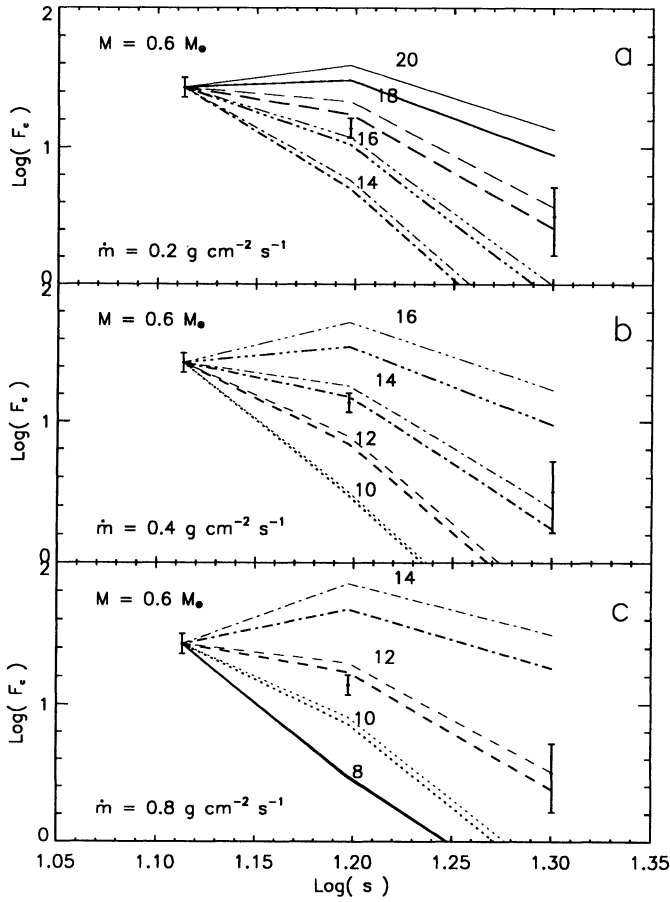


Fig. 5.—Same as Fig. 4 but for $M=0.6\,M_\odot$. The individual curves are for models with magnetic fields of $B_0=8\,\mathrm{MG}$ (solid), $B_0=10\,\mathrm{MG}$ (dotted), $B_0=12\,\mathrm{MG}$ (dash-dotted), $B_0=16\,\mathrm{MG}$ (dash-triple-dotted), $B_0 = 18 \text{ MG}$ (long-dashed), and $B_0 = 20 \text{ MG}$ (solid).

We tested this by setting $r_{dd} = 0$ and keeping all other parameters the same as for Figure 1. Though the light curves did not fit anymore, the resulting range for B_0 only changed by 1 MG. This is because the slope depends mainly on the wavelength, and thus the corresponding s for a given B_0 , where the cyclotron emission turns from being optically thin to being optically thick. In contrast, the slope depends strongly on M, since it determines the shock temperature and since the cyclotron opacities are sensitive to T. That explains the strong dependence of B_0 on M. On the other hand, \dot{m} does not influence the resulting B_0 heavily, since it does not affect T_s and only influences the electron number density and the height of the shock (see

The observations tell us that the peak of the cyclotron radiation is at a lower frequency than that of the I band. This results in an upper limit for B_0 because the cyclotron radiation in the I band must still be at least marginally optically thin. On the other hand, for a B_0 that is too low, the calculated flux decreases too rapidly as one goes from the I band to the V band. For very low B_0 , the free-free opacity becomes larger than the cyclotron opacity and the slope of F_c decreases again. The best fit results for $M=0.4~M_{\odot}$ are $B_0\approx 13-21~MG$ or $\mu=B_0~R^3=1.7\times 10^{34}-2.7\times 10^{34}~G~cm^3$. For $M=0.6~M_{\odot}$, we have $B_0\approx 9-19~MG$ or $\mu=6.0\times 10^{33}-1.3\times 10^{34}~G~cm^3$,

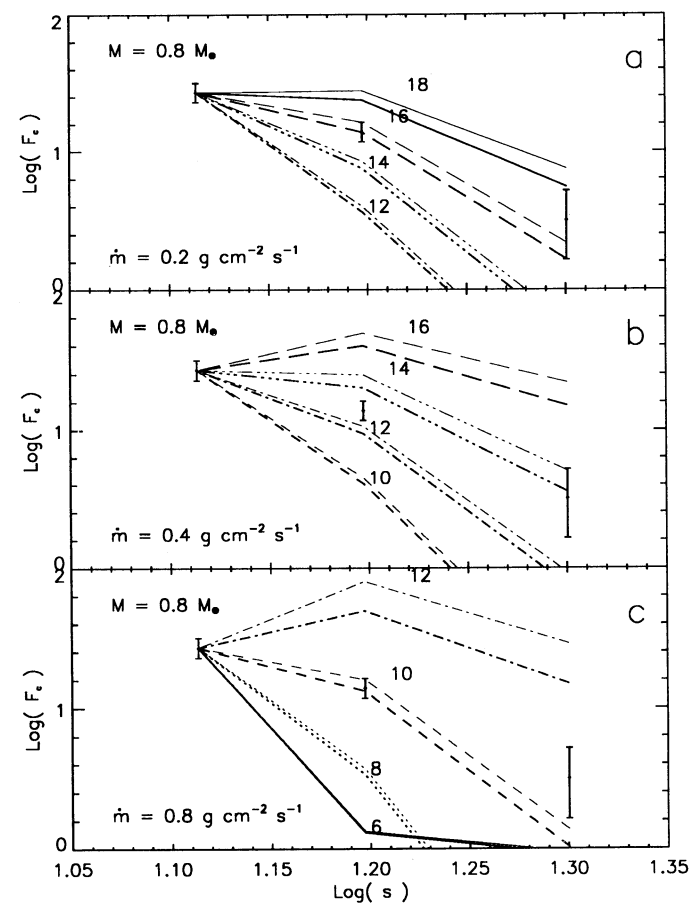


Fig. 6.—Same as Fig. 4 but for $M=0.8~M_{\odot}$. The individual curves are for models with magnetic fields of $B_0=6~\mathrm{MG}$ (solid), $B_0=8~\mathrm{MG}$ (dotted), $B_0=10~\mathrm{MG}$ (dashed), $B_0=12~\mathrm{MG}$ (dash-dotted), $B_0=14~\mathrm{MG}$ (dash-triple-dotted), $B_0=16~\mathrm{MG}$ (long-dashed), and $B_0=18~\mathrm{MG}$ (solid).

and for $M=0.8~M_{\odot}$ we obtain $B_0\approx 9-18~{\rm MG}$ or $\mu=3.2\times 10^{33}-6.4\times 10^{33}~{\rm G~cm}^3$. The results for B_0 for different M and m are also listed in Table 2 together with the magnetic moments, the magnetic radii, and the coupling radii using magnetic fields in between the lower and upper bounds. In order to compare our estimate of B_0 to the estimate of the magnetic field obtained by Piirola et al. (1993), we have to obtain the approximate plasma parameter corresponding to our models. Using the values of x_s and x_s of Table 1 and x_s 0, we obtain x_s 1 and x_s 2 and x_s 3 and x_s 3 and x_s 4 and x_s 3 and x_s 4 and x_s 4 and x_s 5 and x_s 6 and x_s 6 and x_s 7 and x_s 8 and x_s 8 and x_s 9 and x_s 9

than the magnetic field estimate of Piirola et al. (1993) for the corresponding Λ . This is partially a geometric effect, as B_0 is the field strength at the magnetic pole, while the magnetic field strengths in the emission regions are smaller.

4. CONCLUSIONS

An estimate of the magnetic field strength B of the IP RE 0751 + 14 was made by Piirola et al. (1993), who compared the observed maximum circularly polarized flux F_c^{obs} in the I, R, and V band with the calculated flux for uniform temperature models. Here we not only fit quantitatively F_c^{obs} but furthermore use the observed X-ray flux as a constraint for the mass M and the specific accretion rate \dot{m} . The shock structure is also taken into account, so that the temperature and other parameters are not assumed to be uniform. In addition, we require that the same model also fits at least approximately the observed intensity variations at X-ray energies above 10 keV as well as the observed variations of the intensity, the degree of circular and linear polarization, and the position angle in the I band over one spin period. The geometry of the emission regions is based on accretion onto a white dwarf with the magnetic field of a displaced dipole. We obtain the best fits with $B_0 \approx 9-21$ MG or $\mu = 3.2 \times 10^{33}-2.7 \times 10^{34}$ G cm³ for $M = 0.4 - 0.8 M_{\odot}$. A higher M results in a lower B_0 and a lower μ. These values are more characteristic for AM Her systems than for IPs. Furthermore, we find that accretion occurs onto a much smaller fractional surface area of the white dwarf than in a typical IP, as is characteristic of the AM Her binaries. In addition, Ishida (1991) has pointed out that the X-ray modulation amplitude is almost energy independent and that the iron line intensity is modulated with the white dwarf rotation. Both are features common to some AM Her systems.

To summarize, we find that the high magnetic moment that we deduce for RE 0751+14, together with X-ray signatures that are more characteristic of AM Her systems, makes it likely that the white dwarf will synchronize as the system evolves. The existence of IPs which are progenitors of the AM Her binaries had been predicted by Chanmugam & Ray (1984) and King et al. (1985), and RE 0751+14 is the most likely example of such a system known to date.

We thank an anonymous referee for critical comments. This work was supported by NASA grant NAGW 2447 to Louisiana State University and by the Louisiana State Board of Regents in providing funds to establish the Concurrent Computing Laboratory at LSU. The calculations were performed on the MasPar computers at Louisiana State University and at the University of Karlsruhe, Germany.

REFERENCES

Campbell, G. C. 1990, MNRAS, 244, 367
Chanmugam, G. 1992, ARA&A, 30, 143
Chanmugam, G., Frank, J., King, A. R., & Lasota, J.-P. 1990, ApJ, 350, L13
Chanmugam, G., & Ray, A. 1984, ApJ, 285, 252
Cropper, M. 1990, Space Sci. Rev., 54, 195
Frank, J., King, A., & Raine, D. 1992, Accretion Power in Astrophysics, Cambridge Astrophysics Series (Cambridge: Cambridge Univ. Press)
Ishida, M. 1991, Ph.D. thesis, Univ. Tokyo, ISAS Research Note 505
Joss, P. C., Katz, J. I., & Rappaport, S. A. 1979, ApJ, 230, 176
Katz, J. I. 1991, Comments Ap., 15, 177
King, A. R., Frank, J., & Ritter, H. 1985, MNRAS, 213, 181
King, A. R., Frank, J., & Whitehurst, R. 1990, MNRAS, 244, 731
King, A. R., & Shaviv, G. 1984, MNRAS, 211, 883
Lamb, F. K., Aly, J.-J., Cook, M. C., & Lamb, D. Q. 1983, ApJ, 274, L71
Lamb, D. Q., & Patterson, J. 1983, in IAU Colloq. 72, Cataclysmic Variables and Related Objects, ed. M. Livio & G. Shaviv (Dordrecht: Reidel), 229

Mason, K. O., et al. 1992, MNRAS, 258, 749
Meggitt, S. M. A., & Wickramasinghe, D. T. 1982, MNRAS, 198, 71
Nauenberg, M. 1972, ApJ, 175, 417.
Pacholczyk, A. G. 1977, Radio Galaxies (Oxford: Pergamon)
Patterson, J. 1994, PASP, 106, 209
Penning, W. P., Schmidt, G. D., & Liebert, J. 1986, ApJ, 301, 881
Piirola, V., Hakala, P., & Coyne, G. V. 1993, ApJ, 410, L107
Rappaport, S., Verbunt, F., & Joss, P. C. 1983, ApJ, 275, 713
Ritter, H., & Kolb, U. 1995, in X-Ray Binaries, ed. W. H. G. Lewin & E. P. J.
van den Heuvel (Cambridge: Cambridge Univ. Press), in press
Rosen, S. R., Mittaz, J. P. D., & Hakala, P. J. 1993, MNRAS, 264, 171
Rybicki, G. B., & Lightman, A. P. 1979, Radiative Processes in Astrophysics
(New York: Wiley)
Schmidt, G. D., Liebert, J., & Stockman, H. S. 1995, ApJ, 441, 414
Schmidt, G. D., & Stockman, H. S. 1991, ApJ, 371, 749
Spruit, H. C., & Ritter, H. 1983, A&A, 124, 267
Stockman, H. S., Schmidt, G. D., & Lamb, D. Q. 1988, ApJ, 332, 282

Verbunt, F., & Zwaan, C. 1981, A&A, 100, L7

Väth, H. 1994a, Ph.D. thesis, Louisiana State University

——. 1994b, A&A, 284, 319

Väth, H., & Chanmugam, G. 1995, ApJS, 98, 295

Warner, B. 1985, in Interacting Binaries, ed. P. P. Eggleton & J. E. Pringle (Dordrecht: Reidel), 367

West, S. C., Berriman, G., & Schmidt, G. D. 1987, ApJ, 322, L35

Wickramasinghe, D. T. 1988, in Polarized Radiation of Circumstellar Origin, ed. G. V. Coyne, A. M. Magalhães, A. F. J. Moffat, R. E. Schulte-Ladbeck, S. Tapia, & D. T. Wickramasinghe (Vatican City: Vatican Obs.), 1 Wickramasinghe, D. T., & Meggitt, S. M. A. 1985, MNRAS, 214, 605 Wickramasinghe, D. T., Wu, K., & Ferrario, L. 1991, MNRAS, 249, 460 Wu, K., Chanmugam, G., & Shaviv, G. 1994, ApJ, 426, 664 Wu, K., & Wickramasinghe, D. T. 1993, MNRAS, 260, 141